Article

Cell Metabolism

# A Liver-Enriched Long Non-Coding RNA, lncLSTR, Regulates Systemic Lipid Metabolism in Mice

## Graphical Abstract

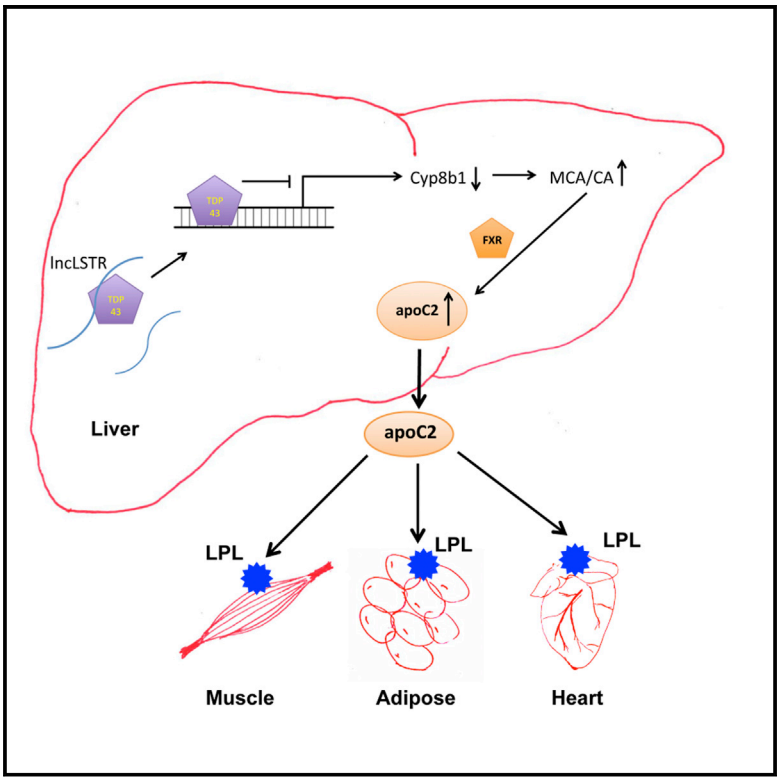


## Authors

Ping Li, Xiangbo Ruan, ..., Jun Zhu, Haiming Cao

## Correspondence

haiming.cao@nih.gov

## In Brief

While the physiological significance of most long non-coding RNAs remains unclear, Li et al. reveal a key role for liver lncLSTR in lipid homeostasis. Together with TDP-43, LncLSTR modifies the bile acid pool to increase FXR-dependent apoC2 expression and activate lipoprotein lipases in peripheral tissues, resulting in enhanced triglyceride clearance.

## Highlights

- A number of lncRNAs enriched in mouse metabolic tissues are identified
- A liver-enriched lncRNA, lncLSTR, regulates triglyceride clearance
- A FXR/apoC2 pathway mediates lncLSTR function in vivo
- A lncLSTR/ TDP-43 complex regulates Cyp8b1 expression and bile profile

Li et al., 2015, Cell Metabolism *21*, 455–467
March 3, 2015 
http://dx.doi.org/10.1016/j.cmet.2015.02.004

Cell Metabolism
Article

# A Liver-Enriched Long Non-Coding RNA, lncLSTR, Regulates Systemic Lipid Metabolism in Mice

Ping Li,[1,5] Xiangbo Ruan,[1,5] Ling Yang,[1,5] Kurtis Kiesewetter,[1] Yi Zhao,[2] Haitao Luo,[2] Yong Chen,[3] Marjan Gucek,[3] Jun Zhu,[4] and Haiming Cao[1,*]
[1]Center for Molecular Medicine, National Heart, Lung and Blood Institute, NIH, Bethesda, MD 20892, USA
[2]Key Laboratory of Intelligent Information Processing, Institute of Computing Technology, Chinese Academy of Sciences, Beijing, PR China
[3]Proteomics Core
[4]Systems Biology Center
National Heart, Lung and Blood Institute, NIH, Bethesda, MD 20892, USA
[5]Co-first author
*Correspondence: haiming.cao@nih.gov
http://dx.doi.org/10.1016/j.cmet.2015.02.004

## SUMMARY

**Long non-coding RNAs (lncRNAs) constitute a significant portion of mammalian genome, yet the physiological importance of lncRNAs is largely unknown. Here, we identify a liver-enriched lncRNA in mouse that we term liver-specific triglyceride regulator (lncLSTR). Mice with a liver-specific depletion of lncLSTR exhibit a marked reduction in plasma triglyceride levels. We show that lncLSTR depletion enhances apoC2 expression, leading to robust lipoprotein lipase activation and increased plasma triglyceride clearance. We further demonstrate that the regulation of apoC2 expression occurs through an FXR-mediated pathway. LncLSTR forms a molecular complex with TDP-43 to regulate expression of Cyp8b1, a key enzyme in the bile acid synthesis pathway, and engenders an in vivo bile pool that induces apoC2 expression through FXR. Finally, we demonstrate that lncLSTR depletion can reduce triglyceride levels in a hyperlipidemia mouse model. Taken together, these data support a model in which lncLSTR regulates a TDP-43/FXR/apoC2-dependent pathway to maintain systemic lipid homeostasis.**

## INTRODUCTION

Mammalian genomes are populated with a large number of long non-coding RNAs (lncRNAs) (Cabili et al., 2011; Guttman et al., 2009; Luo et al., 2013), supporting the concept that the majority of the genome is transcribed (Djebali et al., 2012). LncRNAs are defined as transcripts that are over 200 nt long and lack any coding potential. Most annotated lncRNAs are transcribed from RNA polymerase II and often are capped, spliced, and poly-adenylated (Cabili et al., 2011). The exact number of lncRNAs in genomes is currently unknown and is likely to grow and may equal or even surpass the number of protein-coding genes. The systemic identification of lncRNAs also prompts serious rethinking about the potential nonconventional functions of mRNA. Evolution studies suggest that some mRNAs might arise from lncRNAs (Ulitsky and Bartel, 2013) and therefore might currently carry out important non-coding functions as well. For example, HMGA2 was recently shown to function both as a protein-coding gene and as a non-coding RNA (Kumar et al., 2014). If more mRNAs were confirmed to have similar function, the actual pool of transcripts with lncRNA-like functions might be even much larger than the already documented sizable collections (Ulitsky and Bartel, 2013). LncRNAs are in general less conserved than coding transcripts (Guttman et al., 2009) but have been clearly under selective pressure and often exhibit tissue-specific expression (Cabili et al., 2011), suggesting that they might carry out specific functions. Studies performed in cultured cells have implicated lncRNAs in diverse cellular processes ranging from chromatin modification, RNA stability, to translational control (Batista and Chang, 2013; Clark and Mattick, 2011). A number of reports support a prevailing mechanism for lncRNA action where lncRNAs interact with and organize histone writers, readers, and modifiers (Batista and Chang, 2013; Guttman et al., 2011) to regulate gene transcription, although it remains to be determined whether the majority of lncRNAs function through this mechanism.

The physiological significance of most lncRNAs at whole-organism level is largely unknown, although emerging reports indicate that lncRNAs could play critical roles in essential pathophysiological processes. For example, an lncRNA close to the interferon-λ locus in mice was demonstrated to regulate microbial susceptibility in mice (Gomez et al., 2013). A recent study showed that several lncRNA knockout mice exhibited developmental defects (Sauvageau et al., 2013). Interestingly, significant portions of disease-associated SNPs are distributed in non-coding regions of the human genome (Hindorff et al., 2009), suggesting that lncRNA mutations could be pathogenic. But understanding their contribution to disease also requires careful functional annotation of lncRNAs in animal and human physiology. Of all physiological processes, nutrient sensing and maintenance of metabolic homeostasis are among the most fundamental for life. During fasting or starvation, the body coordinates complex physiological responses to cope with altered nutrient supplies, which are often accompanied by additional changes in the immune and reproductive systems to further promote energy conservation. On the other hand, nutrient excess, manifested clearly by human obesity, often has profound negative impacts on the entire organism, including dyslipidemia, insulin resistance, and tumorigenesis (Calle and Kaaks, 2004;

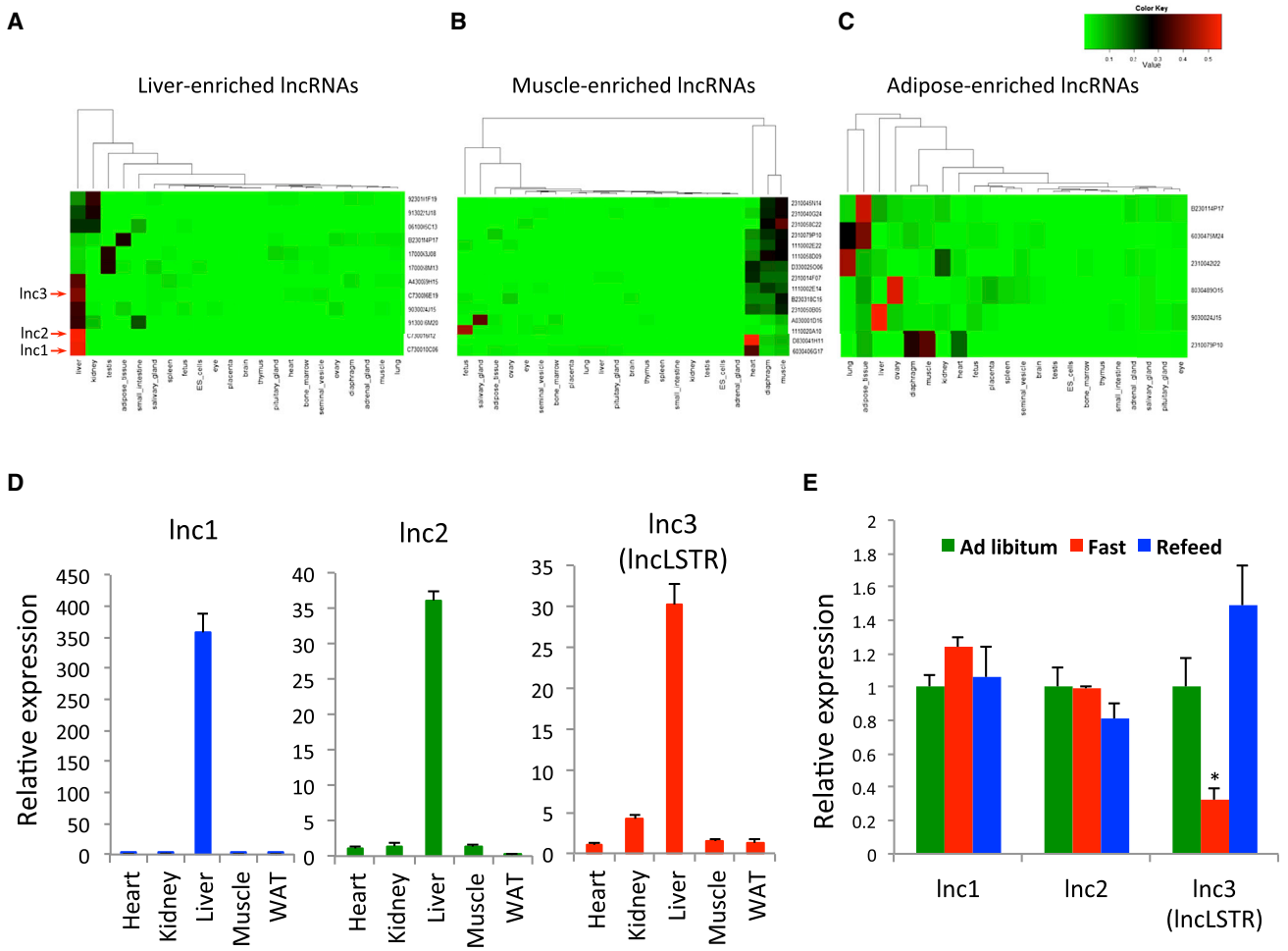


**Figure 1. Identification of a Liver-Enriched lncRNA Regulated by Metabolic State**

(A–C) Graphic presentation of lncRNA transcripts that are enriched in liver (A), muscle (B), and adipose (C) tissues. The color depth represents the expression levels of lncRNAs with red indicating higher expression.

(D) Expression levels of liver-enriched lncRNAs (lncLSTR indicated) in heart, kidney, liver, muscle, and white adipose tissue (WAT) of mice analyzed by quantitative real-time PCR.

(E) Expression levels of liver-enriched lncRNAs in the livers of mice (n = 4) fed ad libitum (Ad libitum), subject to a 24 hr fast (Fast) or a 24 hr fast followed by a 4 hr refeeding (Refeed).

Error bars represent SEM, *p < 0.05.

Eckel et al., 2005). Since lncRNAs are a major unexplored territory of the mammalian genome, and defective energy metabolism is connected to a wide range of pathological conditions, bridging these two essential research areas could significantly contribute to the advance of biology and also open new revenues to therapeutic intervention for diseases. In this study, we have identified a metabolically regulated lncRNA in mouse we named liver-specific triglyceride regulator (lncLSTR), which plays an essential physiological function in mammalian lipid homeostasis.

## RESULTS

### Identification of a Liver-Enriched lncRNA Implicated in Metabolic Regulation

To identify lncRNAs that are potentially involved in systemic metabolism, we first searched for lncRNAs that are enriched in key metabolic organs. By re-annotating the entire collection of probe sets for one of most widely used Affymetrix gene chips, Mouse Genome 430 2.0 Array, we found that 4,571 probes actually target lncRNAs documented in the Fantom 3 database (Liao et al., 2011). Using a dataset of multi-tissue gene expressions profiled with this Affymetrix chip, we identified over 30 lncRNAs that are enriched in liver, muscle, and adipose tissues (Figures 1A–1C and S1A). We initially focused on lncRNAs in the liver, the central nexus of energy metabolism. Among the 12 liver-enriched lncRNAs, three (lnc1–lnc3) exhibit liver-specific expressions (Figure 1A), a pattern that was also confirmed by counting reads of an independent RNA sequencing (RNA-seq) dataset of multiple tissues (Figure S1B). Indeed, all three lncRNAs were shown to be abundantly and predominately expressed in the liver by analyzing our in-house samples (Figure 1D). We reason that if an lncRNA regulates energy metabolism, its expression

level might fluctuate in response to changes in energy levels or metabolic state. In mice subjected to fasting and refeeding, expression levels for one of three liver-enriched lncRNAs (lnc3) has a sharp decline after a 24 hr fast, and it is quickly recovered upon refeeding (Figure 1E). We named this lncRNA liver-specific triglyceride regulator (lncLSTR) based on its function characterized in this report. LncLSTR is an intergenic long non-coding RNA localized in a region of the mouse genome that is syntenic to human chromosome 1q25, yet a clear human homolog could not be immediately identified using the BLAST algorithm (Figures S1C and S6). LncLSTR is a cDNA that was initially characterized in Fantom database (Kawai et al., 2001) and is capped, spliced, and polyadenylated. We used three widely employed algorithms to analyze the protein coding potential for lncLSTR, which all indicate that lncLSTR lacks any coding capacity (Experimental Procedures). In addition, none of the predicated short open reading frames (ORFs) in lncLSTR match any known proteins or functional protein motifs in current proteome databases, further supporting that lncLSTR is a non-coding transcript. Based on these observations, lncLSTR is a liver-enriched lncRNA that is regulated by metabolic milieu in vivo, thereby serving as a potential metabolic regulator in animals.

## LncLSTR Depletion Has Profound Lipid-Lowering Effects in Mice

To directly address the physiological role of lncLSTR in metabolic regulation, we specifically depleted lncLSTR in the liver of mice and studied its impact on energy metabolism. We tested and identified a number of short hairpin RNAs (shRNAs) that could suppress lncLSTR by more than 70% in mouse liver when delivered by recombinant adenoviral vectors (Figure 2A). This system allows us to assess the impact of liver-specific lncLSTR depletion on systemic metabolism. We first profiled essential nutrient factors in the plasma of lncLSTR knockdown (KD) and control mice received lacZ shRNA adenoviruses. There was no difference in plasma ketone, glycerol, or free fatty acid levels between lncLSTR KD and control mice, whereas glucose levels were slightly reduced by lncLSTR depletion (Figure S2A). By contrast, we observed a significant reduction in plasma triglyceride (TG) levels in lncLSTR KD mice compared to controls (Figure 2B). Of note, reduced plasma TG levels in lncLSTR KD mice occurred in all three feeding conditions (Figure 2B). All major phenotypes of lncLSTR depletion were also corroborated with a second pair of shRNA for lncLSTR (Figure S2B), affirming that the metabolic changes we observed were specific to lncLSTR knockdown in mice.

The drastic difference in plasma TG between lncLSTR KD and control mice could be due to impaired intestinal and hepatic TG secretion or enhanced plasma TG clearance by tissue uptake. To distinguish these possibilities, we examined lipid content of fecal excretions in lncLSTR KD and control mice and detected only marginal differences in free fatty acid levels, whereas we found no difference in TG and cholesterol levels between the two groups (Figure S2C). Therefore, differential intestinal absorption is unlikely to be the primary reason for the reduced plasma TG levels in lncLSTR KD mice. Given equal intestinal uptake, plasma TG levels reflect the delicate balance between hepatic secretion and uptake primarily by muscle, adipose, and liver itself. To compare liver TG secretion rates between control and lncLSTR KD mice, we administrated Poloxamer-407, a nonionic detergent that can block TG uptake in mice (Millar et al., 2005), and monitored plasma TG levels for several hours to calculate TG secretion rates. This experiment revealed that TG secretion was not altered by lncLSTR depletion (Figure 2C). Therefore, lncLSTR KD mice very likely have enhanced tissue TG clearance leading to their lower plasma TG levels.

To more vigorously test this idea, we performed a lipid load assay by orally delivering a dose of olive oil into mice and following their plasma TG levels for 4 hr. As expected, control mice exhibited a rapid increase in plasma TG levels that peaked around 2 hr post-administration (Figure 2D). LncLSTR KD mice, however, only showed a marginal increase in their circulating TG that quickly returned to baseline. These data strongly argue that TG clearance is enhanced in mice with liver-specific loss of function of lncLSTR.

Next, we sought to determine whether the lipid-lowering effects of lncLSTR depletion could be exploited to improve disease conditions associated with hyperlipidemia. We tested this idea using a mouse model with a targeted mutation in apolipoprotein E (ApoE). ApoE$^{-/-}$ mice are best known for their hypercholesterolemia but also exhibit significantly elevated triglycerides in circulation, a known contributing factor for their exaggerated atherogenesis (Le and Walter, 2007). Administration of lncLSTR KD adenoviruses into ApoE$^{-/-}$ mice caused no change in their plasma cholesterol levels (Figure S2D) but completely normalized their hypertriglyceridemia, demonstrating that lncLSTR knockdown is also very effective in lowering plasma TG in this disease model (Figure 2E). Hence, liver-enriched lncRNAs such as lncLSTR could potentially be targeted to develop novel therapeutic strategies for the management of hyperlipidemia.

## LncLSTR Depletion Increases ApoC2 Expression and LPL Activities Leading to Enhanced Plasma TG Clearance

Next, we explored the underlying mechanism for the enhanced TG clearance in lncLSTR KD mice. TG clearance from circulation primarily depends on the activities of lipoprotein lipase (LPL) residing in the peripheral tissues such as fat and muscle (Goldberg and Merkel, 2001). When we examined the expression of LPL and other key genes that control TG uptake in these tissues, we found however that they were largely unchanged (Figure S3A). Consistently, post-heparin LPL activities were similar between control and lncLSTR KD mice (Figure S3B). Expression levels of hepatic genes involved in chylomicron and VLDL clearance were also comparable between the two groups (Figure S3A). Consistent with these observations, TG levels in the liver tissues of control and lncLSTR KD mice were indistinguishable (Figure S3E).

The liver is also able to secrete regulatory factors that directly modulate LPL activities without changing their expression levels (Williams, 2008). Such liver-derived LPL regulators include apoC3 and angiopietin-like protein 3 (ANGPTL3), both of which inhibit LPL activity, and apoC2, which is a potent activator of LPL. Expression levels of apoC3 and ANGPTL3 were comparable in lncLSTR KD and control mice, but strikingly there was a very significant increase in apoC2 expression in the liver of

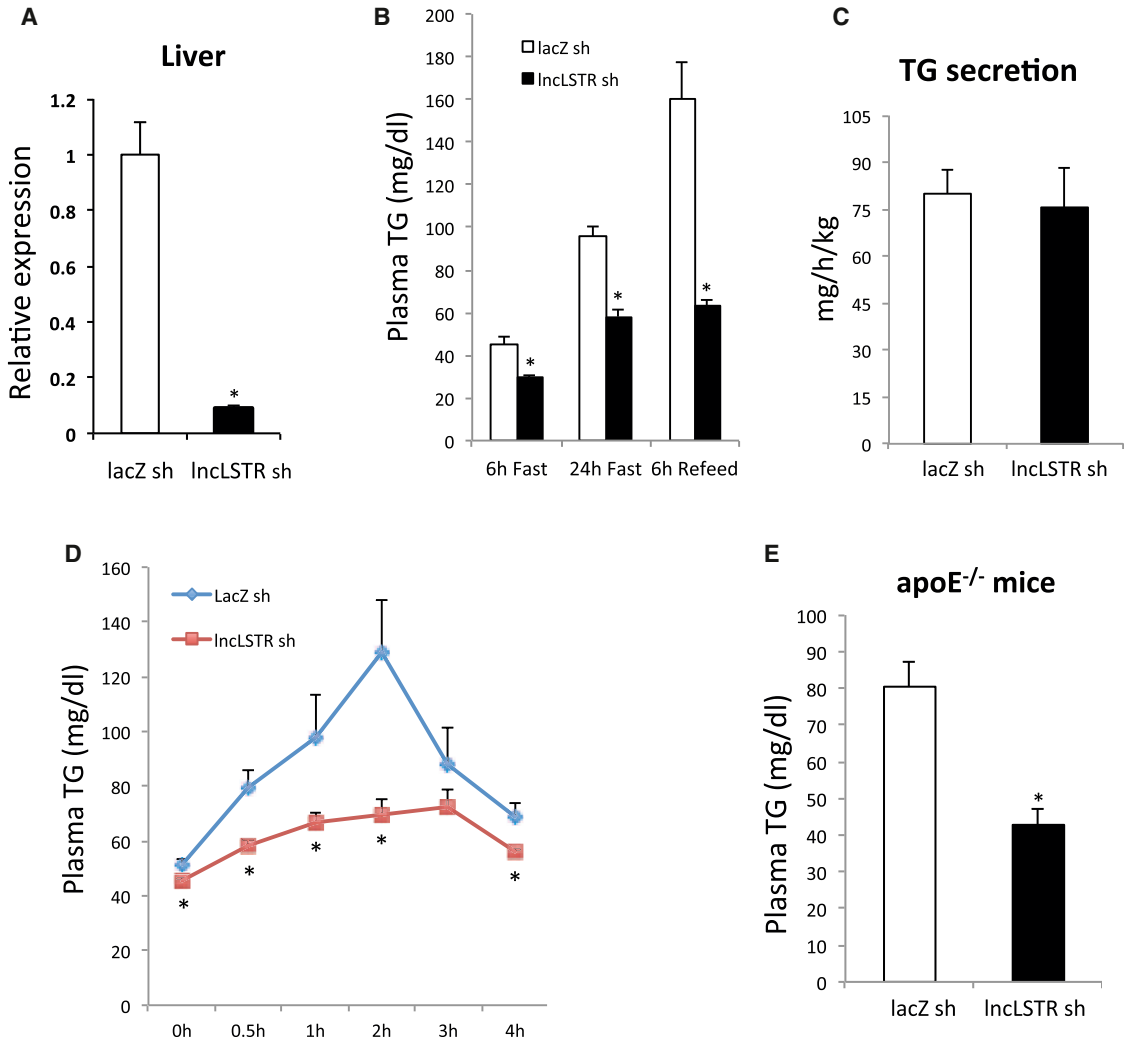


**Figure 2. LncLSTR Knockdown Reduces Plasma TG Levels in Mice**

(A) Expression levels of lncLSTR in the livers of control and lncLSTR KD mice received shRNA adenoviruses for LacZ (LacZ sh) and lncLSTR (lncLSTR sh), respectively (n = 6).

(B) Plasma TG levels in lncLSTR KD (lncLSTR sh) and control (LacZ sh) mice (n = 7) after a 6 hr fast (6h Fast), a 24 hr fast (24h Fast), or 6 hr refeeding after a 24 hr fast (6h Refeed).

(C) TG secretion rates in lncLSTR KD and control mice (n = 6) determined by administration of Poloxamer-407 to block TG uptake.

(D) Plasma TG levels in lncLSTR KD and control mice (n = 7) orally receiving olive oil.

(E) Plasma TG levels in control (n = 8) and lncLSTR KD (n = 7) ApoE$^{-/-}$ mice.

Error bars represent SEM, *p < 0.05.

lncLSTR KD mice (Figures 3A and S2B). Furthermore, plasma apoC2 protein levels were also markedly increased in lncLSTR KD mice compared to controls (Figures 3B and S3C), whereas there was a moderate decrease of apoC1 in the plasma of lncLSTR KD mice and no significant change in protein levels of apoC3, apoE, and Angptl8 (Figure S3C). If the increased apoC2 was indeed a contributing factor for increased peripheral tissue TG clearance in lncLSTR KD mice, we expected that plasma from these mice would be able to activate LPL more efficiently. Indeed, we observed that exogenous LPL activity was strongly elevated in samples mixed with lncLSTR KD mouse plasma compared to controls (Figure 3B). Such robust capacity for activation of LPL will strongly promote systemic TG clearance, resulting in lower circulating levels. To further test this hypothesis, we performed a TG uptake experiment in mice using orally delivered $^{3}$H-triolein and demonstrated that heart, brown fat, and soleus muscle tissues of lncLSTR KD mice exhibit significantly increased uptake of radioactivities than those of control mice, whereas hepatic TG uptake was not changed (Figure S3D). Furthermore, TG levels in soleus muscle during fasting, which are mainly derived from LPL-mediated uptake of TG from VLDLs, were significantly increased in lncLSTR KD mice compared to controls (Figure S3E). To definitively test whether elevated plasma apoC2 is a key factor that leads to enhanced LPL activity

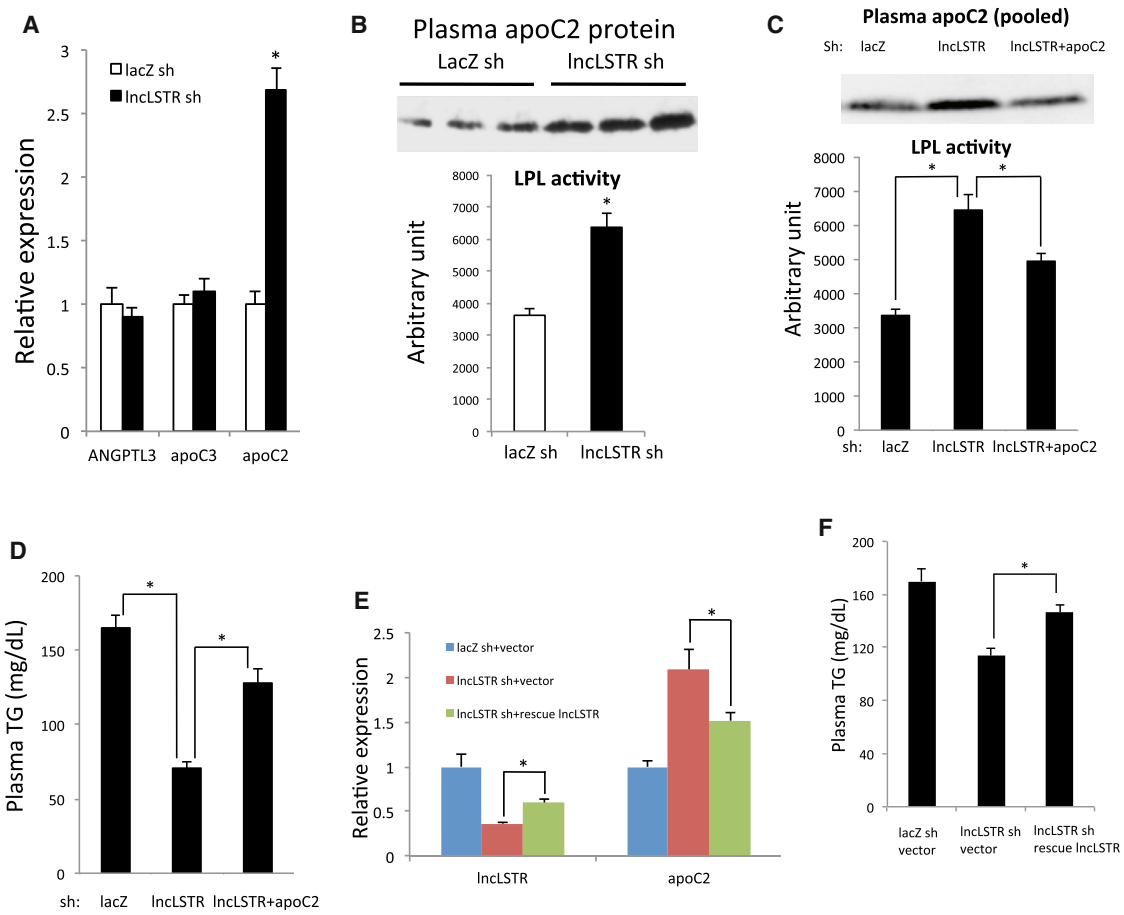


**Figure 3. LncLSTR Regulates ApoC2 Expressions and Plasma LPL-Activating Capacity**

(A) Gene expressions in the livers of control (lacZ sh) (n = 6) and lncLSTR KD (lncLSTR sh) mice (n = 5) after a 6 hr food withdrawal.

(B) Top: plasma apoC2 protein levels in control and lncLSTR KD mice. Plasma from individual mice of each group was analyzed by immunolotting. Bottom: LPL activity stimulation by control or lncLSTR KD mouse plasma (n = 3).

(C) Top: apoC2 protein levels in plasma pooled from 6 mice of each group (control, lncLSTR KD, or lncLSTR and apoC2 double KD mice) were analyzed by immunoblotting. Bottom: LPL activity stimulation by plasma of control, lncLSTR KD, or lncLSTR and apoC2 double KD mice (n = 8).

(D) Plasma TG levels in control (n = 9), lncLSTR KD (n = 10), or lncLSTR and apoC2 double KD mice (n = 9).

(E) Gene expressions in the livers of mice receiving control, lncLSTR KD, or both lncLSTR KD and lncLSTR rescue adenoviruses (n = 6)

(F) Plasma TG levels in mice receiving control, lncLSTR KD, or both lncLSTR KD and lncLSTR rescue adenoviruses (n = 9).

Error bars represent SEM, *$p < 0.05$.

and TG clearance in lncLSTR KD mice, we further knocked down hepatic apoC2 by adenovirus-delivered apoC2 shRNA in lncLSTR KD mice, which reversed the increased apoC2 level in lncLSTR KD mice almost to the control level (Figures 3C and S3F). This strategy effectively diminished the difference in LPL activity stimulated by lncLSTR KD mouse plasma versus controls (Figure 3C). More importantly, it caused a sizable rebound of the reduced plasma TG levels associated with lncLSTR knockdown (Figure 3D).

To gain further insights into the significance of lncLSTR transcript per se in regulating systemic TG metabolism and apoC2 expression, we performed a "rescue" experiment. Basically, we injected lncLSTR KD adenoviruses to suppress endogenous transcripts and concurrently rescued lncLSTR expression by delivering a truncated lncLSTR that lacks the target sequence for the shRNA (Figure S3G). In this system, the expression level of lncLSTR could be significantly increased as compared to lncLSTR KD mice (Figure 3E). Meanwhile, both decreased plasma triglyceride and increased apoC2 expression in lncLSTR knockdown mice were largely reversed as well (Figures 3E and 3F). Therefore, plasma TG appears to be inversely proportional to the levels of apoC2 modulated by lncLSTR under all conditions we have tested.

Taken together, these results strongly support that elevated hepatic and plasma apoC2 levels are indeed an essential underlying reason that lncLSTR depletion increases plasma TG clearance.

## LncLSTR Regulates ApoC2 Expression and Plasma TG Clearance through an FXR-Mediated Pathway

To understand the mechanism by which lncLSTR regulates apoC2 expression, we knocked down lncLSTR in primary

A

| | | |
|---|---|---|
| lncLSTR | mmu00983 Drug metabolism - other enzymes | 4.58E-09 |
| lncLSTR | mmu00830 Retinol metabolism | 8.71E-09 |
| lncLSTR | mmu00982 Drug metabolism - cytochrome P450 | 5.01E-08 |
| lncLSTR | mmu00980 Metabolism of xenobiotics by cytochrome P450 | 8.25E-08 |
| lncLSTR | mmu01100 Metabolic pathways | 2.12E-07 |
| lncLSTR | mmu04976 Bile secretion | 3.39E-06 |
| lncLSTR | mmu00120 Primary bile acid biosynthesis | 3.76E-06 |
| lncLSTR | mmu00053 Ascorbate and aldarate metabolism | 4.63E-06 |
| lncLSTR | mmu04610 Complement and coagulation cascades | 6.17E-06 |

Correlation analysis based on 2425 samples

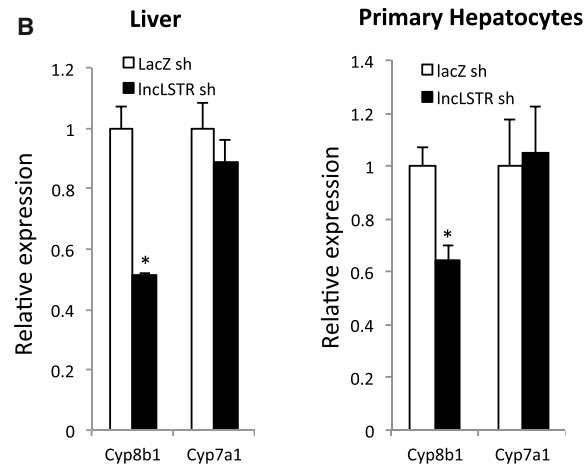


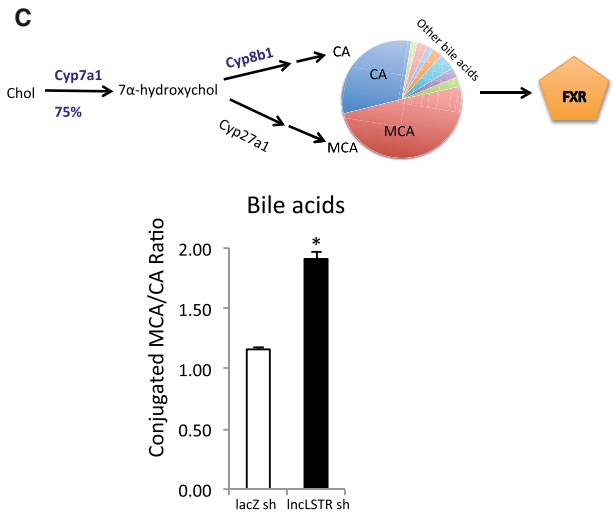


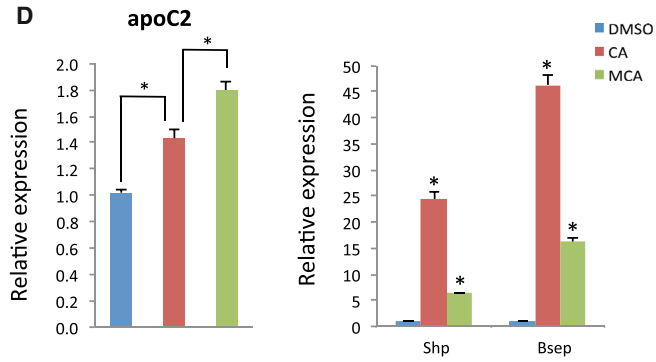


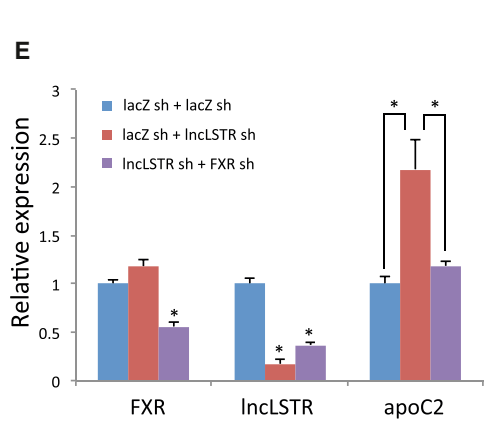


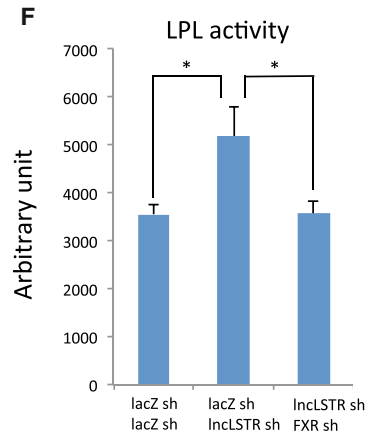


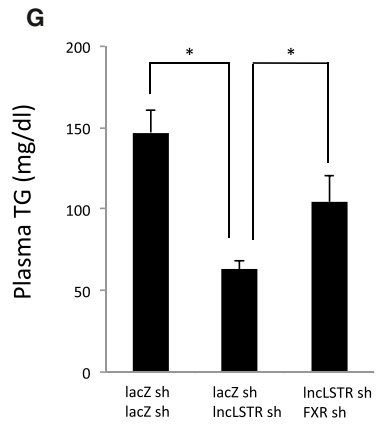


**Figure 4. LncLSTR Regulates ApoC2 through an FXR-Mediated Pathway**

(A) Biological processes identified in a correlation analysis of lncLSTR with coding genes based on 2,425 gene expression samples profiled with Affymetrix Mouse Genome 430 2.0 Array. p value denotes the significance of gene enrichment in annotation terms.

(B) Cyp8b1 and Cyp7a1 expression in the livers of control and lncLSTR KD mice (left, n = 6) or in primary hepatocytes infected with control or lncLSTR KD adenoviruses (right, n = 4).

(C) Top: illustration of bile acid synthesis pathway. Bottom: ratios of conjugated MCA/CA in the gallbladders of control or lncLSTR KD mice. Results represent pooled bile from four mice.

(D) Gene expression in cultured hepatocytes treated with DMSO (control), CA, or MCA.

*(legend continued on next page)*

hepatocytes but found that apoC2 levels were not changed in this setting (Figure S5A), suggesting that lncLSTR does not directly regulate apoC2 through a cell-autonomous mechanism. To identify molecular mediators that might link lncLSTR to apoC2 expression, we employed a similar bioinformatic analysis that initially allowed us to identify lncLSTR as an lncRNA metabolic regulator. Since lncLSTR is one of the targets on the Affymetrix Mouse Genome 430 2.0 Array, its expression levels had already been documented alongside all coding genes in the over one thousand microarray datasets using this chip that have been deposited in the NCBI GEO database. The vast collection of lncLSTR-mRNA coexpression information allowed us to perform extensive correlation analyses to map potential physiological pathways regulated by lncLSTR. Using this analysis, we found that lncLSTR is implicated in multiple metabolic pathways (Figure 4A). In particular, lncLSTR is potentially involved in drug, xenobiotics, and bile acid metabolism. Interestingly, these pathways are intrinsically connected and their proper functioning depends on each other (Modica et al., 2009). Upon careful inspection of the gene list generated by the bioinformatics analysis (Figure S4), we found that Cyp8b1, one of two rate-limiting enzymes in bile acid synthesis, is among the genes whose expression correlates with lncLSTR. Seventeen enzymes catalyze bile acid synthesis, and two of them are very critical and actively regulated. Cyp7a1 mediates the commitment step for 75% of all bile acids, thereby controlling the bile pool size, whereas Cyp8b1 activity determines the ratio of two most abundant bile acids in mouse, cholic acid (CA), and muricholic acid (MCA), thereby controlling bile pool composition (de Aguiar Vallim et al., 2013; Russell, 2009; Thomas et al., 2008) (Figure 4C, bile acid pathway). Consistent with our correlation analysis, we found that Cyp8b1, but not Cyp7a1, was significantly reduced in the livers of lncLSTR KD mice (Figures 4B and S2B). We further examined additional key enzymes of bile acid synthesis pathway residing in different subcellular organelles including Cyp27a1 (Mitochondria), Cyp39a1 (Endoplasmic reticulum), Akr1d1 (Cytoplasm), and Baat (Peroxisome) and found that their mRNA levels were largely not changed except a slight decrease of Cyp27a1 in lncLSTR KD mice (Figure S5B), suggesting that the overall bile acid synthesis pathway is largely intact. Furthermore, we found that Cyp8b1 was also significantly reduced in primary hepatocytes in which lncLSTR was acutely depleted (Figure 4B), suggesting that Cyp8b1 is one of the immediate response genes downstream of lncLSTR and is potentially one of direct targets of lncLSTR.

The significant reduction in Cyp8b1 in lncLSTR KD mice predicts a shift of the MCA/CA ratio of the bile acid pool (Figure 4C, bile acid pathway). In addition to functioning as detergents which facilitate lipid absorption, bile acids also possess diverse biological activities through activation of endogenous nuclear receptors (de Aguiar Vallim et al., 2013). The major bile acid receptor in the liver is FXR, which mediates most of the biological effects of bile acids on glucose and lipid metabolism (Zhang and Edwards, 2008). Interestingly, FXR is also one of the best-characterized regulators of apoC2 expression (Kast et al., 2001). Since each bile acid activates FXR with different potency (de Aguiar Vallim et al., 2013), a significantly altered bile composition in lncLSTR KD mice could potentially increase apoC2 expression through modulating FXR activity. To test this hypothesis, we profiled bile acids in the gallbladder of lncLSTR KD and control mice to reveal a sizeable increase in the ratio of conjugated MCA versus CA in lncLSTR KD mice (Figure 4C).

To understand how such a shift in bile acid ratio could affect FXR activity and apoC2 expression, we treated cultured hepatocytes with MCA or CA and found that both can increase expression of classical FXR targets such as Shp and Bsep (Figure 4D). Intriguingly, MCA has lesser stimulatory effects on these genes than CA, suggesting that MCA is actually a weaker FXR ligand. However, we found that while apoC2 expression in hepatocytes treated with MCA or CA increases, those treated with MCA have significantly stronger enhancement (Figure 4D), which is dependent on FXR (Figure S5C). Therefore, we have observed a ligand-specific, differential transcriptional regulation by FXR in which MCA-stimulated FXR appears to preferentially enhance apoC2 expression compared to when FXR is stimulated by CA.

Finally, to definitively test whether the specific FXR activation of apoC2 expression is a key effector of lncLSTR on TG clearance, we simultaneously knocked down both FXR and lncLSTR in mice and found that the elevated apoC2 in lncLSTR KD mice was diminished when FXR was also reduced (Figures 4E and S5D). FXR knockdown also reversed the capability of lncLSTR KD mouse plasma to activate LPL (Figure 4F). Most importantly, FXR knockdown effectively blunted the lipid-lowering effect of lncLSTR depletion in mice (Figure 4G). To further investigate the significance of FXR function in regulating systemic TG metabolism by lncLSTR, we tested how lncLSTR affects plasma TG levels in FXR null mice. Consistent with the results of FXR knockdown, diminished effects of lowering plasma TG and increasing apoC2 expression by lncLSTR KD were observed in FXR null mice (Figures S5E and S5F). These results lend strong support to our hypothesis that FXR activity and increased apoC2 expression are essential to the enhanced TG clearance in lncLSTR KD mice.

## LncLSTR Interacts with TDP-43 to Regulate Cyp8b1 Expression

We next sought to understand how lncLSTR regulates Cyp8b1 expression. First, we performed fractionation of mouse liver tissue and found that lncLSTR is enriched in the nucleus (Figure 5A), suggesting a potential role in gene transcription. Many lncRNAs involved in transcription regulation often function through specific protein binding partners, especially histone modifiers (Guttman et al., 2011). We then performed an RNA pull-down using nuclear extracts of liver tissues to identify proteins that interact with lncLSTR. Several additional bands were present in the SDS-PAGE silver staining analysis of the fraction precipitated with biotin-labeled lncLSTR compared to an antisense control (Figure 5B). Proteins in these specific bands were identified by

(E) Hepatic gene expressions in mice receiving control, lncLSTR KD, or both FXR and lncLSTR KD adenoviruses (n = 5).
(F) LPL activities stimulated by plasma of mice receiving control, lncLSTR KD, or both FXR and lncLSTR KD adenoviruses (n = 5).
(G) Plasma TG levels in mice receiving control, lncLSTR KD, or both FXR and lncLSTR KD adenoviruses (n = 9).
Error bars represent SEM, *$p < 0.05$.

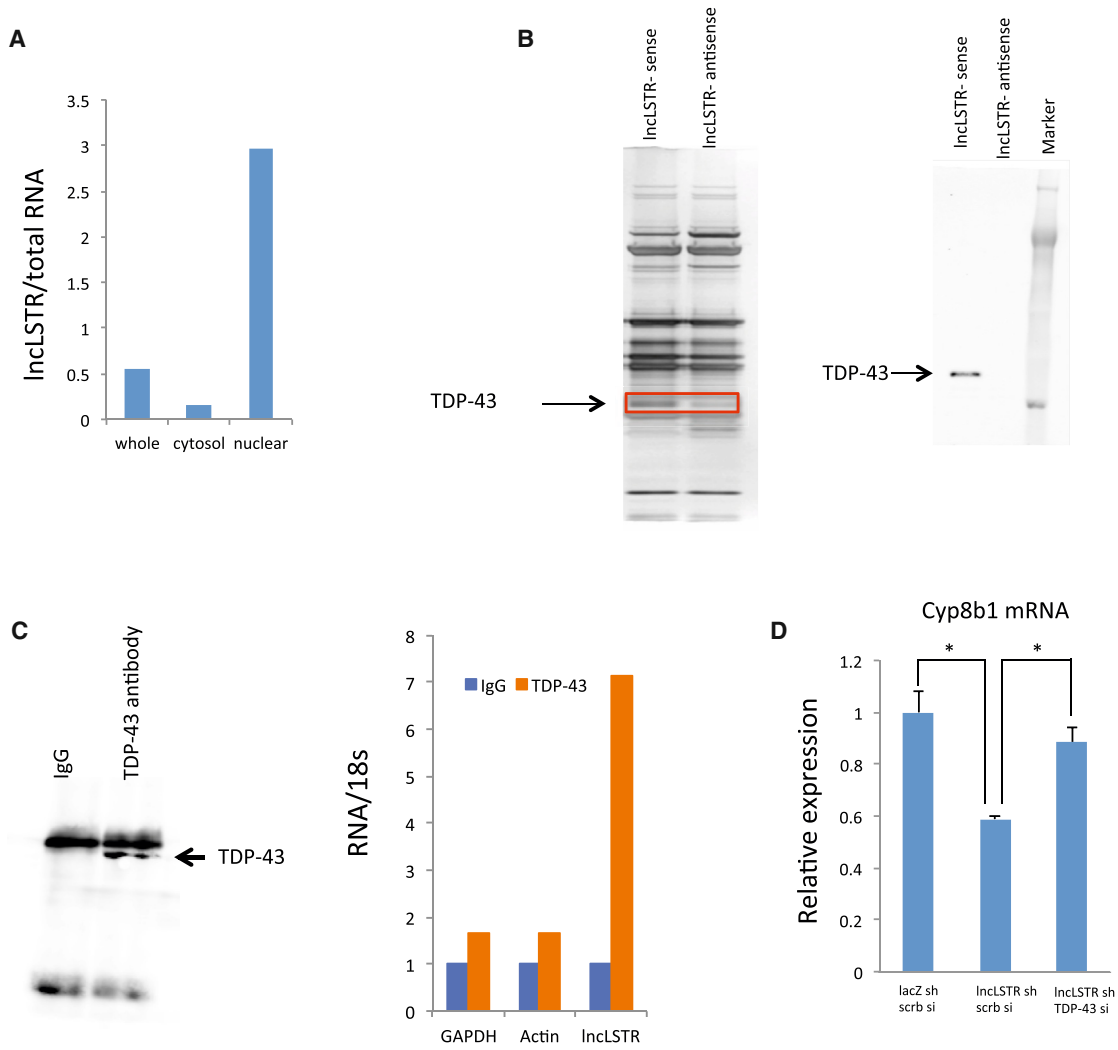


**Figure 5. LncLSTR Interacts with TDP-43**

(A) Levels of lncLSTR in whole-cell, cytosolic, or nuclear fractions of liver tissues pooled from 4 mice.

(B) Left: silver-stained SDS-PAGE gel analysis of proteins in nuclear extract of liver tissues that are bound to biotinylated lncLSTR or its antisense. The highlighted regions were analyzed by mass spectrometry, identifying TDP-43 as a protein unique to lncLSTR. Right: immunoblotting analysis of proteins in nuclear extract of liver tissues that are bound to biotinylated lncLSTR or its antisense using an anti-TDP-43 antibody.

(C) Left: anti-TDP-43 immunoblotting analysis of proteins in immunoprecipitates of liver tissues using an anti-TDP-43 antibody. Right: glyceraldehyde 3-phosphate dehydrogenase (GAPDH), actin, and lncLSTR RNA levels in immunoprecipitates of liver tissues using an anti-TDP-43 antibody.

(D) Cyp8b1 expression in primary hepatocytes receiving lacZ shRNA, lncLSTR shRNA, scramble siRNA (scrb si), or TDP-43 siRNA in combination as indicated (the Ct levels of Cyp8b1 and TDP-43 are ~27 and ~23, respectively).

Error bars represent SEM, *$p < 0.05$.

mass spectrometry, one of which was TDP-43, a known RNA and DNA binding protein (Lee et al., 2012). We confirmed the specific interaction between TDP-43 and lncLSTR by immunoblotting the lncLSTR-associated proteins with an antibody specific to TDP-43 (Figure 5B). To test whether the lncLSTR-TDP-43 interaction also occurs in vivo, we performed reciprocal pulldown of TDP-43 using liver tissue (Figure 5C) and quantified RNAs in the immunoprecipitates using quantitative real-time PCR. These experiments revealed that lncLSTR is significantly enriched in anti-TDP-43 precipitate but not in the IgG control (Figure 5C).

We next asked whether TDP-43 is functionally involved in the regulation of Cyp8b1 expression by lncLSTR. TDP-43 knockdown, when performed in combination with lncLSTR KD in primary hepatocytes, completely reversed the reduced Cyp8b1 expression associated with lncLSTR depletion (Figures 5D and S5G). TDP-43 often acts as a transcriptional suppressor when bound to DNA (Lee et al., 2012). Thus, it is possible that TDP-43 binds to and inhibits the Cyp8b1 promoter and that this inhibitory effect can be relieved when complexed with lncLSTR. To test this hypothesis, we co-expressed TDP-43 with a Cyp8b1 promoter-driven luciferase construct in HEK293 cells and

demonstrated that the Cyp8b1 promoter activity induced by HNF4α was suppressed by nearly 40% in the presence of TDP-43 (Figure 6A). Interestingly, when lncLSTR was also present, the inhibitory effect of TDP-43 on Cyp8b1 promoter was significantly diminished (Figure 6A).

To further understand the molecular basis that TDP-43 regulates Cyp8b1 expression, we took steps to map the TDP-43-responsive locus on the Cyp8b1 promoter. We tested truncated Cyp8b1 promoters ranging from 1,800 to 200 bp and found that a 200 bp proximal Cyp8b1 promoter can still be suppressed by TDP-43 (Figure 6B). To determine whether TDP-43 directly binds to Cyp8b1 promoter, we performed a binding assay using recombinant TDP-43 proteins and a biotinylated 200 bp DNA fragment of the Cyp8b1 promoter. These results demonstrate that TDP-43 directly interacts with the Cyp8b1 promoter without the need of accessory proteins (Figure 6C). Subsequently, we localized the TDP-43 binding site on Cyp8b1 promoter to a short 40 bp region (−200 to −160) by screening several truncated versions of the original 200 bp promoter (Figure 6D). Finally, to determine whether lncLSTR also regulates TDP-43 binding to Cyp8b1 promoter in vivo, we performed chromatin immunoprecipitation of liver tissues using a specific TDP-43 antibody and demonstrated that TDP-43 binds to the Cyp8b1 promoter (Figure 6E). Intriguingly, TDP-43 binding to the Cyp8b1 promoter was clearly enhanced when lncLSTR was depleted (Figure 6E), further confirming that the inhibitory effect of TDP-43 on Cyp8b1 promoter is also subject to the regulation of lncLSTR in vivo.

Based on these observations, we propose that interaction of TDP-43 with lncLSTR reduces its occupancy and inhibition of the Cyp8b1 promoter. Depletion of lncLSTR leads to increased binding of TDP-43, reduced Cyp8b1 gene expression, and a substantial change in bile acid composition. The altered bile acids activate FXR to increase apoC2 levels, resulting in enhanced TG clearance in mice (Figure 6F).

## DISCUSSION

In recent years, lncRNAs have been being continuously discovered at an unprecedented pace, yet their physiological significance remains elusive (Derrien et al., 2012; Xie et al., 2014). Mammals use complex hormonal and metabolite networks to allow organs to communicate and to maintain physiological homeostasis. The identification of the regulatory function of lncLSTR in systemic triglyceride metabolism suggests that animals could employ lncRNAs to coordinate metabolic processes in multiple organs. Regulation of TDP-43/Cyp8b1 by lncLSTR consequently impact an FXR/apoC2 pathway to regulate TG clearance, indicating that there might be extensive connections between lncRNAs and the established signaling and metabolic network. FXR activity modulates multiple metabolic pathways including bile acid synthesis and lipid homeostasis (de Aguiar Vallim et al., 2013). Activation of this pathway has pleiotropic beneficial effects in the context of metabolic disorders (Thomas et al., 2008). In addition, TDP-43 is a key regulator of microRNA and mRNA processing aside from being a transcriptional repressor (Lee et al., 2012). Given that FXR deficiency did not completely block the lipid-lowing effects of lncLSTR depletion, the interaction between lncLSTR and TDP-43 might have additional molecular and physiological functions, representing an interesting area for future investigations.

Our study also provides further insights into the role of apoC2 in plasma TG metabolism, particularly its functional significance to LPL activation. It is well documented that patients with homozygous deficiency of apoC2 have elevated TG and significantly reduced LPL activity supporting that apoC2 is an LPL activator (Cox et al., 1978). But this notion was complicated by observations that apoC2 heterozygotes in human often do not exhibit hypertriglyceridemia (Cox et al., 1978; Gabelli et al., 1993), and apoC2 transgenic mice paradoxically have hypertriglyceridemia, potentially due to the blockage of the VLDL and LPL interaction by the high apoC2 levels (Shachter et al., 1994). We have demonstrated that a reversal of the enhanced apoC2 expression in lncLSTR KD mice by liver-specific apoC2 knockdown is sufficient to cause rebound of the reduced plasma TG levels associated with lncLSTR knockdown (Figures 3C and 3D). Consistently, recent reports showed that infusion of recombinant apoC2 in mice results in decrease of TG levels (Lee et al., 2011), and an apoC2 mimetic peptide activates LPL and decreases triglyceride levels in mice (Amar et al., 2015). These results support that apoC2, when regulated within physiological range, positively regulates LPL activities and plasma TG uptake in mice.

In light of thousands of uncharacterized lncRNAs that could also have important physiological functions, our work provides a practical and efficient platform for identification and characterization of functional lncRNAs in crucial physiological processes. It is currently unclear how many lncRNAs are functional, and it is still very challenging to identify functionally important lncRNAs from the large collection of documented non-coding transcripts. These difficulties are partly due to the fact that some lncRNAs could be simple byproducts of pervasive transcription of coding genes. In addition, it is often more difficult to infer function for an lncRNA based on its evolutional history because the current comparative genomic tools cannot easily detect homology between lncRNAs (Ulitsky and Bartel, 2013). We have carried out detailed analyses of human/mouse homology of lncLSTR by analyzing human RNA-seq databases for potential transcripts expressed from the lncLSTR syntenic region in human genome and could not identify a clear human homolog for it (Figure S6). Therefore, it remains to be determined whether a human ''homolog'' of lncLSTR has significantly evolved in its primary sequence yet maintains its structure or function. Nevertheless, it is important to be able to efficiently identify those lncRNAs that are likely to be functional as predicted by a knowledge-based analysis and then to quickly test their function in vivo. Our approach is to correlate lncRNA expression with coding gene expressions within large, established collection of tissue-specific datasets followed by rapid virus-mediated lncRNA knockdown. Our platform can also be adapted to perform tests pre-clinically to determine whether lncRNAs, especially those that have clear human homologs, could constitute therapeutic targets for metabolic disorders. Of course, more studies are needed before the full potential of lncRNAs as a therapy can be assessed. However, considering that most disease-associated SNPs are distributed in non-coding regions of the genome (Hindorff et al., 2009), functionally connecting even a small portion of lncRNAs to specific diseases could generate a paradigm shift on the drug discovery process.

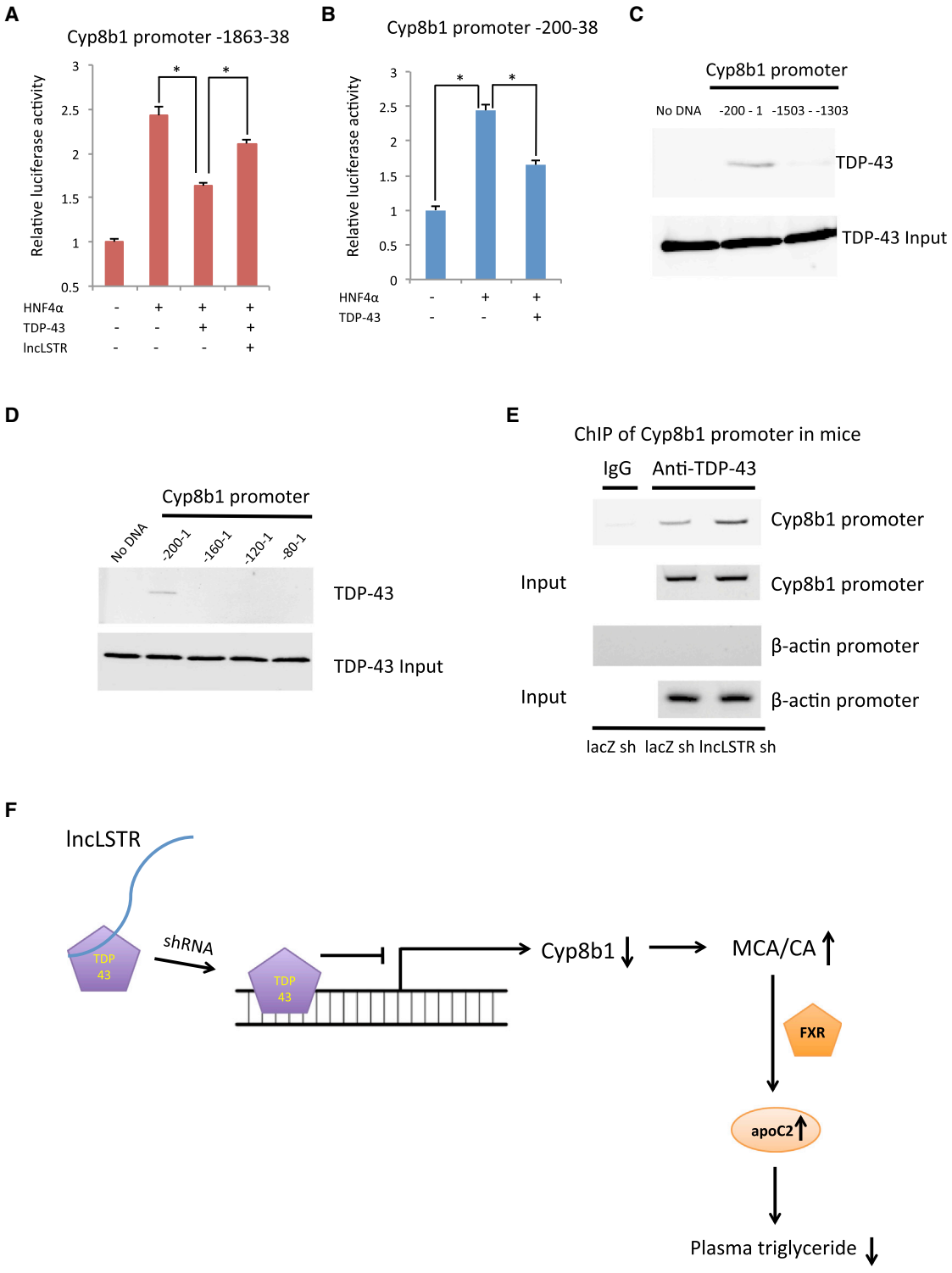


**Figure 6. LncLSTR Interacts with TDP-43 to Regulate Cyp8b1 Expression**

(A) Cyp8b1 promoter-driven luciferase activities in cells transfected with HNF4α expression vector in combination with vectors expressing either TDP-43 or lncLSTR. Negative control for HNF4α and TDP-43 is a pcDNA 6.2 vector expressing a yellow fluorescent protein, and negative control for lncLSTR is the empty pcDNA 6.2 vector.

(B) Luciferase activities driven by Cyp8b1 promoter (200 bp) in cells transfected with HNF4α expression vector in combination with vectors expressing either TDP-43 or YFP control.

(C) In vitro binding of biotinylated Cyp8b1 promoter (−200–1) with recombinant TDP-43. A biotinylated Cyp8b1 promoter fragment (−1,503–1,303) was used as a negative control.

*(legend continued on next page)*

In summary, our work reveals a novel lncRNA signaling pathway that operates in a physiological context. We also provide a framework for future identification and functional annotation of lncRNAs in systemic metabolism and other crucial physiological processes. Of note, our bioinformatics analyses have revealed that key metabolic organs such as muscle and adipose also specifically express a number of lncRNAs. A critical objective for the future would be to elucidate the potential interactions and integrations of these lncRNAs to coordinate metabolic responses.

## EXPERIMENTAL PROCEDURES

### Bioinformatic Analyses

Mouse multi-tissue expression data (GSE9954, NCBI GEO database), which measured gene expression in 22 mouse tissues using the Affymetrix Mouse Genome 430 2.0 Array with two to three replicates for each tissue, was used to identify mouse liver enriched lncRNAs. The microarray data were re-annotated based on the annotation of Fantom 3 and Refseq databases using the preprocessing method "MAS5" run by ncFANs (http://www.bioinfo.org/ncfans/) to obtain expression profiles containing 14,861 coding genes and 4,571 lncRNAs (Liao et al., 2011). Briefly, for the total 496,468 probes in the Mouse 430 2.0 array, only those perfectly matching to a transcript in the non-coding sequences of Fantom 3 or coding sequences in Refseq database were retained, giving rise to two sets of probes that targeted coding and non-coding transcripts. We also removed the non-coding probes that matched coding cDNA sequences in both the Refseq database and FANTOM3 project. After these filtering processes, 67,089 probes (13.5%) perfectly matched the FANTOM3 non-coding RNAs but not any Refseq mouse coding transcript, and 248,116 probes (50.0%) matched Refseq coding transcripts but not any non-coding RNAs. We also removed an additional 39,775 probes (8.0%) that matched both Refseq coding transcripts and FANTOM3 lncRNAs. To further reduce the noise, we removed probes matching more than one gene, and to increase the accuracy, we discarded genes that were targeted by less than three probes, leaving 14,861 coding genes and 5,169 non-coding genes. To obtain an even more reliable set of non-coding genes, we removed non-coding genes with a Codon Substitution Frequency score <300, as well as those lncRNA loci whose genomic region could not be transformed from the mm5 to mm9 of the mouse genome sequence release. Finally, 14,861 coding genes and 4,571 lncRNA genes were retained. On average, coding and non-coding genes were targeted by 14.9 and 11.2 probes, respectively. The tissue enrichment of lncRNA expression was evaluated by Shannon Entropy, the measurement of information content occurred as directed in order to identify tissue-specific coding genes (Zhang and Zhang, 2011). As the information content (tissue-enrichment) of a transcript increases, its entropy decreases. The lncRNAs with overall expression entropy less than three and with categorical expression entropy for each tissue less than four were considered to be tissue-specific lncRNAs. The mean Fragments Per Kilobase of transcript per Million (FPKM) for each liver-enriched lncRNAs were calculated based on a RNA-seq dataset of six different mouse tissues including heart, hippocampus, liver, lung, spleen, and thymus (Keane et al., 2011).

The protein-coding potential of lncLSTR sequence was evaluated by three widely used algorithms, Coding Potential Calculator (CPC) (Kong et al., 2007), Coding-Non-Coding Index (CNCI) (Sun et al., 2013), and Coding Potential Assessment Tool (CPAT) (Wang et al., 2013). For CPC, transcripts with scores more than 1 are classified as "coding," less than −1 as "non-coding," and between −1 and 1 are marked as "weak non-coding"([−1, 0]) or "weak coding"([0, 1]), respectively. The CPC score of lncLSTR is −1.12249, which was calculated with http://cpc.cbi.pku.edu.cn/programs/run_cpc.jsp using default thresholds. For CNCI, the transcripts with scores more than 0 are classified as coding while less than 0 are non-coding. The CNCI score of lncLSTR is −1.59, indicating that it is a non-coding RNA. For CPAT, mouse coding probability (CP) cutoff is 0.44, so transcripts with scores more than 0.44 are classified as "coding" and less than 0.44 as "non-coding." The coding potential of lncLSTR calculated with http://lilab.research.bcm.edu/cpat/index.php using default thresholds is 0.38, also indicating that it is a non-coding transcript.

We scanned lncLSTR from both directions to identify all putative open reading frames (ORFs) over 150 bp using ATG as start codon and TAA, TAG, TAG as stop codons, and found five short ORFs, none of which are over 300 bp, the cutoff for lncRNAs. We then used the putative ORFs to search protein databases including all non-redundant GenBank CDS translations+PDB+SwissProt+PIR+PRF, excluding environmental samples of unknown sources from WGS projects, and found no match to any known protein. Finally, we searched these putative ORFs against the Conserved Domain Database (http://www.ncbi.nlm.nih.gov/Structure/bwrpsb/bwrpsb.cgi) and did not find any match.

2,425 individual samples from 34 Affymetrix Mouse Genome 430 2.0 Array datasets deposited in NCBI GEO database (http://www.ncbi.nlm.nih.gov/geo/) were used to construct a "two-color" co-expression network including both coding and non-coding genes with an established method (Guo et al., 2013) to predict potential biological processes in which lncLSTR might be involved. Each of the 34 datasets consists of nine or more different experimental conditions or cellular states, which include a number of biochemical and biophysical conditions, various tissue resources, and diverse biological processes. The accession numbers of datasets used in this analysis are GSE8582, GSE8307, GSE8249, GSE7759, GSE7012, GSE6678, GSE6595, GSE6514, GSE6487, GSE5976, GSE5296, GSE4051, GSE1986, GSE1479, GSE1435, GSE13149, GSE12769, GSE11923, GSE11222, GSE10871, GSE10493, GSE10246, GSE10765, GSE11922, GSE6065, GSE12982, GSE13765, GSE11056, GSE9954, GSE9809, GSE9630, GSE9442, GSE9338, and GSE4288.

### Adenovirus Production and In Vivo Adenovirus Administration

The shRNAs for lncLSTR, FXR, and apoC2 were designed to act against mouse sequences (lncLSTR shRNA1: 5′-GTTGGAAGCTCTAAATAAA-3′, shRNA2: 5′-GACGATTGCTACATGTATA-3′; FXR shRNA: 5′-GTGTAAATCT AAACGGCTA-3′; apoC2 shRNA: 5′-TCCCTTCCTGCCACTACAT-3′). The hairpin template oligonucleotides were synthesized by Integrated DNA Technologies and were subsequently cloned into the adenovirus vector of the pAD/Block-it system (Invitrogen) according to the manufacturer's protocols. Rescue construct of lncLSTR was generated by PCR-amplifying a truncated lncLSTR that lack 299 bp at 5′ end carrying the shRNA1 target sequence, and it was subsequently cloned into pAdv5 adenovirus vector for virus packaging. Adenoviruses were amplified in HEK293A cells and purified by CsCl gradient centrifugation. Purified viruses were desalted with PD10 columns (GE Healthcare Life Sciences) and titered with Adeno-X Rapid Titer Kit (Clontech). Adenoviruses were delivered into mice intravenously at 1–2 × $10^9$ pfu/mouse. In the case of double knockdown experiments, two viruses of equal titer were first mixed, then each mouse received 2 × $10^9$ pfu total virus. After 7 to 12 days, animal experiments were performed, and tissue samples and plasma were harvested for further analysis.

### Triglyceride Secretion

Mice were fasted for 6 hr. In vivo secretion rates of triglyceride (TG) into plasma were determined in conscious, unrestrained mice, following intraperitoneal injection of 1 g/kg body weight Poloxamer 407 (P-407, Sigma). Immediately before, at 60 min, and 120 min after P-407 administration, tail vein blood samples were taken for TG level measurement with a colorimetric assay system (Sigma) adapted for microplate format. TG secretion rates were calculated using the slope between 60 min and 120 min, based on the assumption of a plasma volume of 3.5% of body weight.

(D) In vitro binding of biotinylated Cyp8b1 promoter fragments as indicated with recombinant TDP-43.
(E) Chromatin immunoprecipitation of liver tissues of control and lncLSTR KD mice using an anti-TDP-43 antibody. Bands were amplified with specific primers for Cyp8b1 (targeting −392 to 1) or β-actin promoters.
(F) A working model where lncLSTR regulates a TDP-43/FXR/apoC2 pathway to control plasma TG clearance in mice.
Error bars represent SEM, *$p < 0.05$.

### Oral Lipid Tolerance Test

Mice were fasted for 4 hr and then received 0.2 ml olive oil by oral gavage. Blood was taken from the tail vein right before and at different time points after the oil load (0 min, 30 min, 1 hr, 2 hr, 3 hr, and 4 hr) to measure total triglyceride levels in the blood by using the device and triglyceride strips from Cardiochek.

### Plasmid Constructs and Reporter Assay

The full-length TDP-43 was amplified from mouse liver cDNA and inserted into the pcDNA6.2 mammalian expression vector (Invitrogen). A yellow fluorescent protein (YFP) cDNA was cloned into the same vector as a control. A plasmid carrying lncLSTR was purchased from B-Bridge International and lncLSTR was sub-cloned into pcDNA6.2. Cyp8b1 promoters with different lengths were amplified by PCR using mouse genomic DNA and cloned into a promoterless pcDNA6.2 vector with a firefly luciferase reporter. HEK293A cells were maintained in DMEM medium supplemented with 10% CCS. Cells were transfected with Cyp8b1 reporter, HNF4$\alpha$ (Plasmid 33006, Addgene), lncLSTR, and TDP-43 or YFP vectors, using polyethylenimine (PEI), and the luciferase assay was performed 24 hr later using the Dual-Luciferase Reporter Assay Kit (Promega). Transfection efficiency was measured by normalization to Renilla luciferase activity expressed from a co-transfected pTK-RL vector (Promega).

### RNA Pull-Down Assay and Native RNA Immunoprecipitation

The RNA pull-down was performed as described previously (Rinn et al., 2007). Briefly, biotin-labeled RNAs were in vitro transcribed using the Biotin RNA Labeling Mix and T7 RNA polymerase (Ambion), and purified with the RNeasy Mini Kit (QIAGEN) on-column digestion of DNA. To prepare the mouse liver nuclear extract, frozen liver tissues were homogenized using a dounce homogenizer with 15–20 strokes in nuclear isolation buffer (250 mM sucrose, 10 mM Tris-HCl [pH 7.5], 1 mM EDTA with protease inhibitors). Nuclear pellets were collected by centrifugation at 1,000 × *g* for 10 min, resuspended in 1 ml RNA immunoprecipitation (RIP) buffer (150 mM NaCl, 20 mM Tris [pH 7.4], 1 mM EDTA, 0.5% Triton X-100 with protease inhibitors and RNaseOUT). The lysates were mechanically sheared again using a dounce homogenizer with 15–20 strokes. Nuclear membrane and other debris were pelleted by centrifugation at 12,000 rpm for 10 min. The folded sense or anti-sense RNAs (1 ug) were added into 2 mg pre-cleared nuclear lysates (supplemented with 0.2 mg/ml heparin, 0.2 mg/ml yeast tRNA and 1 mM DTT) and incubated at 4°C for 1 hr. Sixty microliters of washed Streptavidin-coupled Dynabeads (Invitrogen) were added to each binding reaction and further incubated at 4°C for 1 hr. Beads were washed briefly five times with RIP buffer and heated at 70°C for 10 min in 1× LDS loading buffer, and the retrieved proteins were visualized by SDS-PAGE and silver staining. The unique protein bands shown in the sense RNA pull-down were identified by Mass Spectrometry. For native RIP, 5 ug anti-TDP43 antibody or rabbit IgG were added into 3 mg precleared liver nuclear lysates and incubated at 4°C for 2 hr. 50 ul Dynabeads Protein G were added and incubated for 1 hr at 4°C with gentle rotation. Beads were washed briefly five times with RIP buffer and resuspended in 1 ml of Trizol. Co-precipitated RNAs were isolated and analyzed by RT-PCR.

### Recombinant Protein Binding Assay

400 ng biotin-labeled Cyp8b1 promoter fragments and 1 ug recombinant TDP-43 protein (OriGene, TP310639) were incubated in 300 ul binding buffer (0.1 mg/ml BSA, 10 ng/ul sperm DNA (Sigma, D7656), 5% glycerol, 0.5 mM DTT, 20 mM HEPES,50 mM KCl,1 mM MgCl2, 0.2% NP-40) for 30 min at 25°C. 30 ul streptavidin beads were added into the binding reaction and incubated for another 30 min. Beads were washed briefly four times with binding buffer and boiled in 1× SDS loading buffer, and the retrieved proteins were visualized by SDS-PAGE and western blot.

### Chromatin Immunoprecipitation Analysis

Chromatin immunoprecipitation (ChIP) assays of frozen liver tissue were performed using a Simple ChIP Enzymatic Chromatin IP kit (Cell Signaling Technology) according to the manufacturer's protocol. Immunoprecipitation was performed using an anti-TDP-43 antibody (ab41881) from Abcam or with rabbit IgG as a negative control. Primers used for amplifying Cyp8b1 and β-actin promoters are: Cyp8b1-chip-f, 5′-TTAGAGACGAGGAAAGAGA TGTGTACA-3′; Cyp8b1-chip-r, 5′-CAGCGCTGGAATTGCTTTATG-3′; Actin-chip-f, 5′-GCTTCTTTGCAGCT CCTTCGTTG-′3; Actin-chip-r, 5′-TTTGCACA TGCCGGAGCCGTTGT-3′. The PCR cycle parameters were 95°C for 5 min, then 30 cycles of 95°C for 30 s, 60°C for 30 s, and 72°C for 45 s, followed by a final extension at 72°C for 5 min for both of ChIP product and input (represent ~0.2%). PCR products were resolved by electrophoresis in a 2% Agarose E-gel (Invitrogen).

### Statistical Analysis

Values represent mean ± SEM. Statistical significance of differences was determined by Student's t test or one-way ANOVA with Bonferroni's post hoc comparison where appropriate. p values less than 0.05 were considered to be significant.

## SUPPLEMENTAL INFORMATION

Supplemental Information includes Supplemental Experimental Procedures, six figures, and one table and can be found with this article online at http://dx.doi.org/10.1016/j.cmet.2015.02.004.

## AUTHOR CONTRIBUTIONS

P.L., X.B.R., and L.Y. designed the study, performed the experiments, analyzed the data, wrote the manuscript, and contributed equally. K.K., Y.C., M.G., and J.Z. performed the experiments. Y.Z. and H.T.L. performed the bioinformatics analyses. H.C. conceived and supervised the study and wrote the manuscript.

## ACKNOWLEDGMENTS

This work was supported by the Division of Intramural Research of the National Heart Lung and Blood Institute (HL006103 and HL006159) of the NIH, USA. Y.Z. and H.L. were supported by a grant from National Natural Science Foundation of China (No. 31371320).

Received: June 20, 2014
Revised: December 12, 2014
Accepted: February 6, 2015
Published: March 3, 2015

## REFERENCES

Amar, M.J., Sakurai, T., Sakurai-Ikuta, A., Sviridov, D., Freeman, L., Ahsan, L., and Remaley, A.T. (2015). A novel apolipoprotein C-II mimetic peptide that activates lipoprotein lipase and decreases serum triglycerides in apolipoprotein E-knockout mice. J. Pharmacol. Exp. Ther. *352*, 227–235.

Batista, P.J., and Chang, H.Y. (2013). Long noncoding RNAs: cellular address codes in development and disease. Cell *152*, 1298–1307.

Cabili, M.N., Trapnell, C., Goff, L., Koziol, M., Tazon-Vega, B., Regev, A., and Rinn, J.L. (2011). Integrative annotation of human large intergenic noncoding RNAs reveals global properties and specific subclasses. Genes Dev. *25*, 1915–1927.

Calle, E.E., and Kaaks, R. (2004). Overweight, obesity and cancer: epidemiological evidence and proposed mechanisms. Nat. Rev. Cancer *4*, 579–591.

Clark, M.B., and Mattick, J.S. (2011). Long noncoding RNAs in cell biology. Semin. Cell Dev. Biol. *22*, 366–376.

Cox, D.W., Breckenridge, W.C., and Little, J.A. (1978). Inheritance of apolipoprotein C-II deficiency with hypertriglyceridemia and pancreatitis. N. Engl. J. Med. *299*, 1421–1424.

de Aguiar Vallim, T.Q., Tarling, E.J., and Edwards, P.A. (2013). Pleiotropic roles of bile acids in metabolism. Cell Metab. *17*, 657–669.

Derrien, T., Johnson, R., Bussotti, G., Tanzer, A., Djebali, S., Tilgner, H., Guernec, G., Martin, D., Merkel, A., Knowles, D.G., et al. (2012). The GENCODE v7 catalog of human long noncoding RNAs: analysis of their gene structure, evolution, and expression. Genome Res. *22*, 1775–1789.

Djebali, S., Davis, C.A., Merkel, A., Dobin, A., Lassmann, T., Mortazavi, A., Tanzer, A., Lagarde, J., Lin, W., Schlesinger, F., et al. (2012). Landscape of transcription in human cells. Nature *489*, 101–108.

Eckel, R.H., Grundy, S.M., and Zimmet, P.Z. (2005). The metabolic syndrome. Lancet *365*, 1415–1428.

Gabelli, C., Bilato, C., Santamarina-Fojo, S., Martini, S., Brewer, H.B., Jr., Crepaldi, G., and Baggio, G. (1993). Heterozygous apolipoprotein C-II deficiency: lipoprotein and apoprotein phenotype and RsaI restriction enzyme polymorphism in the Apo C-IIPadova kindred. Eur. J. Clin. Invest. *23*, 522–528.

Goldberg, I.J., and Merkel, M. (2001). Lipoprotein lipase: physiology, biochemistry, and molecular biology. Front. Biosci. *6*, D388–D405.

Gomez, J.A., Wapinski, O.L., Yang, Y.W., Bureau, J.F., Gopinath, S., Monack, D.M., Chang, H.Y., Brahic, M., and Kirkegaard, K. (2013). The NeST long ncRNA controls microbial susceptibility and epigenetic activation of the interferon-γ locus. Cell *152*, 743–754.

Guo, X., Gao, L., Liao, Q., Xiao, H., Ma, X., Yang, X., Luo, H., Zhao, G., Bu, D., Jiao, F., et al. (2013). Long non-coding RNAs function annotation: a global prediction method based on bi-colored networks. Nucleic Acids Res. *41*, e35.

Guttman, M., Amit, I., Garber, M., French, C., Lin, M.F., Feldser, D., Huarte, M., Zuk, O., Carey, B.W., Cassady, J.P., et al. (2009). Chromatin signature reveals over a thousand highly conserved large non-coding RNAs in mammals. Nature *458*, 223–227.

Guttman, M., Donaghey, J., Carey, B.W., Garber, M., Grenier, J.K., Munson, G., Young, G., Lucas, A.B., Ach, R., Bruhn, L., et al. (2011). lincRNAs act in the circuitry controlling pluripotency and differentiation. Nature *477*, 295–300.

Hindorff, L.A., Sethupathy, P., Junkins, H.A., Ramos, E.M., Mehta, J.P., Collins, F.S., and Manolio, T.A. (2009). Potential etiologic and functional implications of genome-wide association loci for human diseases and traits. Proc. Natl. Acad. Sci. USA *106*, 9362–9367.

Kast, H.R., Nguyen, C.M., Sinal, C.J., Jones, S.A., Laffitte, B.A., Reue, K., Gonzalez, F.J., Willson, T.M., and Edwards, P.A. (2001). Farnesoid X-activated receptor induces apolipoprotein C-II transcription: a molecular mechanism linking plasma triglyceride levels to bile acids. Mol. Endocrinol. *15*, 1720–1728.

Kawai, J., Shinagawa, A., Shibata, K., Yoshino, M., Itoh, M., Ishii, Y., Arakawa, T., Hara, A., Fukunishi, Y., Konno, H., et al.; RIKEN Genome Exploration Research Group Phase II Team and the FANTOM Consortium (2001). Functional annotation of a full-length mouse cDNA collection. Nature *409*, 685–690.

Keane, T.M., Goodstadt, L., Danecek, P., White, M.A., Wong, K., Yalcin, B., Heger, A., Agam, A., Slater, G., Goodson, M., et al. (2011). Mouse genomic variation and its effect on phenotypes and gene regulation. Nature *477*, 289–294.

Kong, L., Zhang, Y., Ye, Z.Q., Liu, X.Q., Zhao, S.Q., Wei, L., and Gao, G. (2007). CPC: assess the protein-coding potential of transcripts using sequence features and support vector machine. Nucleic Acids Res. *35*, W345–W349.

Kumar, M.S., Armenteros-Monterroso, E., East, P., Chakravorty, P., Matthews, N., Winslow, M.M., and Downward, J. (2014). HMGA2 functions as a competing endogenous RNA to promote lung cancer progression. Nature *505*, 212–217.

Le, N.A., and Walter, M.F. (2007). The role of hypertriglyceridemia in atherosclerosis. Curr. Atheroscler. Rep. *9*, 110–115.

Lee, J.H., Giannikopoulos, P., Duncan, S.A., Wang, J., Johansen, C.T., Brown, J.D., Plutzky, J., Hegele, R.A., Glimcher, L.H., and Lee, A.H. (2011). The transcription factor cyclic AMP-responsive element-binding protein H regulates triglyceride metabolism. Nat. Med. *17*, 812–815.

Lee, E.B., Lee, V.M., and Trojanowski, J.Q. (2012). Gains or losses: molecular mechanisms of TDP43-mediated neurodegeneration. Nat. Rev. Neurosci. *13*, 38–50.

Liao, Q., Liu, C., Yuan, X., Kang, S., Miao, R., Xiao, H., Zhao, G., Luo, H., Bu, D., Zhao, H., et al. (2011). Large-scale prediction of long non-coding RNA functions in a coding-non-coding gene co-expression network. Nucleic Acids Res. *39*, 3864–3878.

Luo, H., Sun, S., Li, P., Bu, D., Cao, H., and Zhao, Y. (2013). Comprehensive characterization of 10,571 mouse large intergenic noncoding RNAs from whole transcriptome sequencing. PLoS ONE *8*, e70835.

Millar, J.S., Cromley, D.A., McCoy, M.G., Rader, D.J., and Billheimer, J.T. (2005). Determining hepatic triglyceride production in mice: comparison of poloxamer 407 with Triton WR-1339. J. Lipid Res. *46*, 2023–2028.

Modica, S., Bellafante, E., and Moschetta, A. (2009). Master regulation of bile acid and xenobiotic metabolism via the FXR, PXR and CAR trio. Front Biosci (Landmark Ed) *14*, 4719–4745.

Rinn, J.L., Kertesz, M., Wang, J.K., Squazzo, S.L., Xu, X., Brugmann, S.A., Goodnough, L.H., Helms, J.A., Farnham, P.J., Segal, E., and Chang, H.Y. (2007). Functional demarcation of active and silent chromatin domains in human HOX loci by noncoding RNAs. Cell *129*, 1311–1323.

Russell, D.W. (2009). Fifty years of advances in bile acid synthesis and metabolism. J. Lipid Res. *50*, S120–S125.

Sauvageau, M., Goff, L.A., Lodato, S., Bonev, B., Groff, A.F., Gerhardinger, C., Sanchez-Gomez, D.B., Hacisuleyman, E., Li, E., Spence, M., et al. (2013). Multiple knockout mouse models reveal lincRNAs are required for life and brain development. eLife *2*, e01749.

Shachter, N.S., Hayek, T., Leff, T., Smith, J.D., Rosenberg, D.W., Walsh, A., Ramakrishnan, R., Goldberg, I.J., Ginsberg, H.N., and Breslow, J.L. (1994). Overexpression of apolipoprotein CII causes hypertriglyceridemia in transgenic mice. J. Clin. Invest. *93*, 1683–1690.

Sun, L., Luo, H., Bu, D., Zhao, G., Yu, K., Zhang, C., Liu, Y., Chen, R., and Zhao, Y. (2013). Utilizing sequence intrinsic composition to classify protein-coding and long non-coding transcripts. Nucleic Acids Res. *41*, e166.

Thomas, C., Pellicciari, R., Pruzanski, M., Auwerx, J., and Schoonjans, K. (2008). Targeting bile-acid signalling for metabolic diseases. Nat. Rev. Drug Discov. *7*, 678–693.

Ulitsky, I., and Bartel, D.P. (2013). lincRNAs: genomics, evolution, and mechanisms. Cell *154*, 26–46.

Wang, L., Park, H.J., Dasari, S., Wang, S., Kocher, J.P., and Li, W. (2013). CPAT: Coding-Potential Assessment Tool using an alignment-free logistic regression model. Nucleic Acids Res. *41*, e74.

Williams, K.J. (2008). Molecular processes that handle — and mishandle — dietary lipids. J. Clin. Invest. *118*, 3247–3259.

Xie, C., Yuan, J., Li, H., Li, M., Zhao, G., Bu, D., Zhu, W., Wu, W., Chen, R., and Zhao, Y. (2014). NONCODEv4: exploring the world of long non-coding RNA genes. Nucleic Acids Res. *42*, D98–D103.

Zhang, Y., and Edwards, P.A. (2008). FXR signaling in metabolic disease. FEBS Lett. *582*, 10–18.

Zhang, Z., and Zhang, M.Q. (2011). Histone modification profiles are predictive for tissue/cell-type specific expression of both protein-coding and microRNA genes. BMC Bioinformatics *12*, 155.